

The influence of van der Waals forces on droplet morphological transitions and solvation forces in nanochannels

F. Dutka¹ and M. Napiórkowski²

¹*Institute of Physical Chemistry, Polish Academy of Sciences, ul. Kasprzaka 44/52, 01-224 Warszawa, Poland*

²*Institute of Theoretical Physics, Faculty of Physics, University of Warsaw, ul. Hoża 69, 00-681 Warszawa, Poland*

(Dated: 24 August 2021)

The morphological phase transition between a sessile and lenticular shapes of a droplet placed in a nanochannel is observed upon increasing the droplet volume. The phase diagram for this system is discussed within the macro- and mesoscopic approaches. On the mesoscopic level, the van der Waals forces are taken into account via the effective interface potential acting between the channel walls and the droplet. We discuss the contact angle dependence on the droplet volume and the distance between the walls; this angle turns out to be smaller than the macroscopic Young's angle. The droplet presence induces the solvation force acting between the channel walls. It can be both attractive and repulsive, depending on the width of the channel.

PACS numbers: 47.60.Dx, 68.03.Cd, 68.05.-n, 68.65.-k, 83.50.Ha

Keywords: nanofluidics, phase transitions, van der Waals forces, line tension, solvation forces

I. INTRODUCTION

The progress in miniaturization of microfluidic systems brings new challenges for the theoretical description of such systems. The behavior and manipulation of liquid droplets or gas bubbles (called the discrete phase) in a planar channel of micrometer size filled with immiscible continuous phase is rather well understood^{1,2}. In the absence of electrostatic interactions and neglecting the gravity (which plays minor role on these scale) the droplet can be described by the macroscopic theory^{3,4}.

When the size of the channel becomes smaller and its height is below 100 nm, the droplet shape cannot be described by the macroscopic theory; one has to take into account the long-ranged van der Waals forces. They give rise to the effective interaction between the walls of the channel and the droplet surface^{5,6}. In our mesoscopic description we consider droplets which do not touch the walls of the channel, and a thin layer of continuous phase separating the walls and the droplet is present⁷. This type of morphologies will be investigated in the following analysis. Fabrication of nanochannels and filling them with liquid is already experimentally feasible^{8,9}; carbon nanotubes are good examples of such nanocapillaries^{10,11}.

The influence of the effective interface potential on the shape of the droplets in rectangular and circular capillaries has been usually investigated in two regions^{5,6,12–17}. One region corresponds to the droplet surface close to the walls of the channel where the disjoining pressure dominates. The second region corresponds to droplet surface located in the center of the capillary where the effect of disjoining pressure on the shape of the droplet can be ignored.

In our mesoscopic analysis we investigate the channel heights in the range 10-100 nm and determine the influence of the effective interface potential on droplet shape for any position of the droplet surface. We discuss in de-

tail the geometry of the droplets, such as the thickness of the layer between the droplet and the walls of the channel, as well as the change of the apparent contact angle as function of the increasing height of the channel.

Many of the previous papers on the shapes of the droplets in microchannels have focused on the droplets which were spread between the walls of the channel^{18–21}. In the present analysis we put stress on the morphological transition between the sessile state (the droplet touching only one wall of the channel) and the lenticular state (the droplet touching both walls of the channel). The phase diagrams displaying this transition are presented and discussed, in Section II for the macroscopic approach and in Section III for the mesoscopic approach. In Section IV we point at the role of the line tension when comparing the macroscopic and mesoscopic approaches. We also discuss the solvation force^{22,23} which emerges between the channel walls, Section V. It turns out that both in macroscopic and mesoscopic approaches the sign of this force changes upon increasing the channel width, turning from repulsive to attractive. We show that the solvation force is zero in situation when the droplet can be inscribed in the circle whose center coincides with the symmetry point of the droplet. Section VI contains discussion.

II. MACROSCOPIC DESCRIPTION

On the macroscopic level one can distinguish three generic equilibrium shapes of the *A*-fluid droplet placed in a flat channel filled with *B*-fluid, see Fig. 1. For simplicity, we consider a quasi-two dimensional system which is translationally invariant in one direction. By the shape of the droplet we mean the shape of its cross section perpendicular to the direction in which the system is translationally invariant. Three different morphological states of the droplet can be characterized by the number of

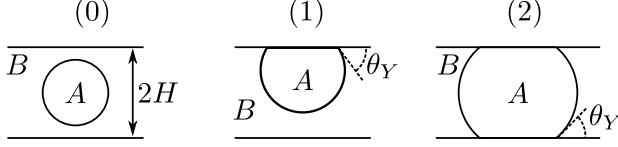


FIG. 1. Three generic macroscopic states of an A -fluid droplet in a planar channel filled with the B -fluid. The droplet can touch zero (0), one (1) or two (2) walls, and the macroscopic states are denoted accordingly. The distance between the walls is $2H$.

walls it remains in contact with: (0), the droplet doesn't touch any of the walls; (1), the droplet touches only one wall, and (2), the droplet touches both walls. In all three cases the shape of the droplet can be described by an arc of a circle. In case (0) the droplet forms a full circle and this state is called the circular state. In the case (1) the shape is a circular segment and we call it the sessile state. The state (2) is called the lenticular (lens-shaped) state. Whenever the AB interface touches the wall it forms with it an apparent contact angle θ_Y . We note that generically by the contact angle one means the angle between the droplet interface and the wall, i.e. $\pi - \theta_Y$. Here we use the angle θ_Y to stress that one of the typical experimental realizations of such a system is the channel filled with liquid (the B -fluid) and its vapor represents the A -fluid. So, the angle θ_Y is the angle formed by the droplet of liquid (B) deposited on a planar wall in ambient conditions (A). We shall often refer to the Young's equation

$$\cos \theta_Y = \frac{\gamma_{WA} - \gamma_{WB}}{\gamma}, \quad (1)$$

where γ_{WA} , γ_{WB} , and γ are the wall- A fluid, wall- B fluid, and A -fluid - B -fluid surface tension coefficients, respectively. We consider the angles $0 \leq \theta_Y \leq \pi/2$ which is the most common situation in droplet microfluidics^{1,2}.

We assume that the fluids A and B are immiscible and incompressible such that the bulk free energy of the system with a droplet relative to the energy of the channel completely filled by the phase B depends neither on the shape nor on the position of the droplet. It depends only on the cross-sectional area A to which we shall often refer to as the droplet's volume. To track the morphological phase transitions we analyze only the surface free energies, which for the above three states are given by:

$$\begin{aligned} \Omega_0 &= 2\gamma\sqrt{\pi}\sqrt{A}, \\ \Omega_1 &= 2\gamma\sqrt{\pi - \theta_Y + \sin \theta_Y \cos \theta_Y}\sqrt{A}, \\ \Omega_2 &= 2\gamma H \left(\frac{\pi - 2\theta_Y}{2 \cos \theta_Y} + \sin \theta_Y + \frac{1}{2} \cos \theta_Y \frac{A}{H^2} \right). \end{aligned} \quad (2)$$

We notice that the energy of the circular state is always larger than the one corresponding to the sessile state,

$\Omega_0 > \Omega_1$. There are thus two competing equilibrium states: sessile and lenticular. If however, the circular states are imposed on the system, e.g., via the constraint on the droplet to be placed symmetrically with respect to the center plane of the channel, then one also allows for the circular - lenticular transition.

For large enough volumes A the lenticular state has lowest surface energy, see Figs 2, 3. The equations

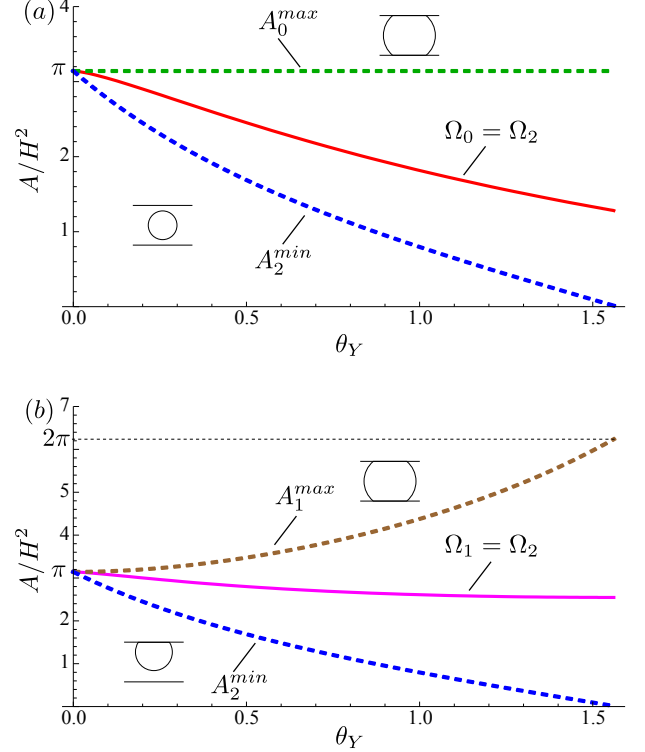


FIG. 2. The phase diagrams illustrating the circular-lenticular (a), and the sessile-lenticular (b) first-order transitions. The phase diagrams are plotted in the contact angle θ_Y and the volume A variables. The solid lines denote the coexistence curves and the dashed lines are the spinodals. The surface energies (Ω_0 , Ω_1 , Ω_2) and volumes (A_0^{max} , A_1^{max} , A_2^{min}) are given in Eq. (2) and Eq. (3), respectively.

$\Omega_0 = \Omega_2$ and $\Omega_1 = \Omega_2$ determine the coexistence curves. The circular, sessile, and lenticular states cease to exist for areas $A_0 > A_0^{max}$, $A_1 > A_1^{max}$, $A_2 < A_2^{min}$, respectively, which are given by:

$$\begin{aligned} A_0^{max} &= \pi H^2, \\ A_1^{max} &= H^2 \frac{4}{(1 + \cos \theta_Y)^2} (\pi - \theta_Y + \sin \theta_Y \cos \theta_Y), \\ A_2^{min} &= H^2 \left(\frac{\pi - 2\theta_Y}{\cos^2 \theta_Y} - 2 \tan \theta_Y \right), \end{aligned} \quad (3)$$

and determine the spinodal curves.

The free energy profiles corresponding to the circular - lenticular and the sessile - lenticular transitions are plot-

ted as function of A/H^2 for the special choice of $\theta_Y = \pi/4$ in Fig. 3a and Fig. 3b, respectively. On these figures the

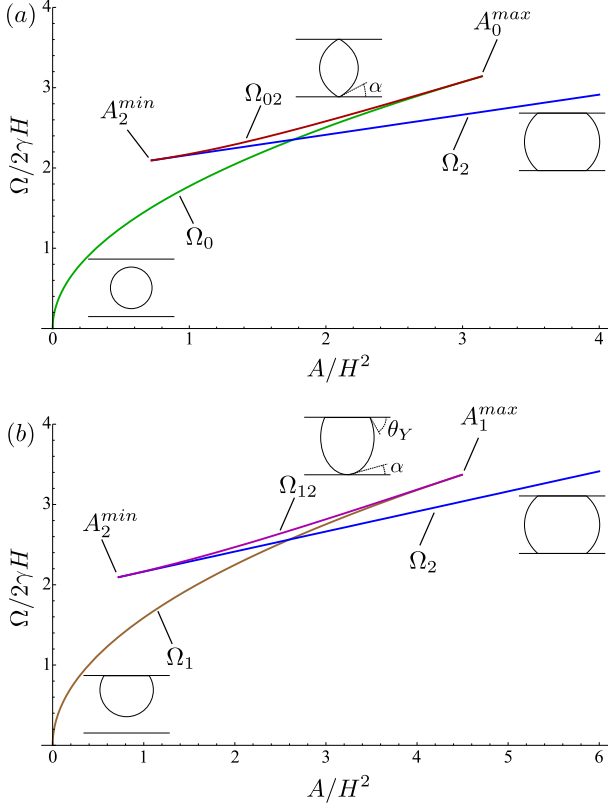


FIG. 3. Surface energy Ω as a function of an area A for the circular-lenticular (a), and sessile-lenticular (b) transitions for $\theta_Y = \pi/4$. The surface energies (Ω_0 , Ω_1 , Ω_2) and areas (A_0^{max} , A_1^{max} , A_2^{min}) are given in Eq. (2) and Eq. (3), respectively. The symbols Ω_{02} and Ω_{12} (Eq. (4)) denote the energies of a continuum of unstable states which connect smoothly spinodal points. The angle α characterizing unstable states changes between $0 \leq \alpha \leq \theta_Y$.

spinodal points are connected by the lines consisting of particularly constructed unstable states whose morphologies interpolate smoothly between the stable states. The free energies and volumes of these states are denoted by Ω_{02} and A_{02} for the circular – lenticular transition, and Ω_{12} and A_{12} for the sessile – lenticular transition. The unstable morphologies can be characterized by only one parameter, the contact angle α which changes from $0 \leq \alpha \leq \theta_Y$, see Fig. 3. For $\alpha = \theta_Y$ one has $A_{02} = A_2^{min}$ and $A_{12} = A_2^{min}$ (the lenticular state), while for $\alpha = 0$

the volume $A_{02} = A_0^{max}$ for the circular – lenticular transition, and $A_{12} = A_1^{max}$ for the sessile – lenticular transition. The free energies of these particular unstable states are given by

$$\begin{aligned} \Omega_{02} &= 2\gamma H \frac{\pi - 2\alpha}{\cos \alpha}, \\ \Omega_{12} &= 2\gamma H \frac{2(\pi - \theta_Y - \alpha + \cos \theta_Y (\sin \theta_Y - \sin \alpha))}{\cos \theta_Y + \cos \alpha}. \end{aligned} \quad (4)$$

One could think about other choice of unstable states but these proposed here are characterized by only one parameter and they smoothly interpolate between the spinodal points on Fig. 3. It turns out that such unstable states appear also in the mesoscopic description.

III. MESOSCOPIC DESCRIPTION

A. Equilibrium shape of the droplet

We assume the system to be translationally invariant in the y -direction and due to the invariance of the confining walls in the x direction the equilibrium shape of the droplet has to be symmetric with respect to axis parallel to the z -axis. We fix this symmetry axis at $x = 0$ and place the walls of the channel at $z = H$, and $z = -H$ (Fig. 4).

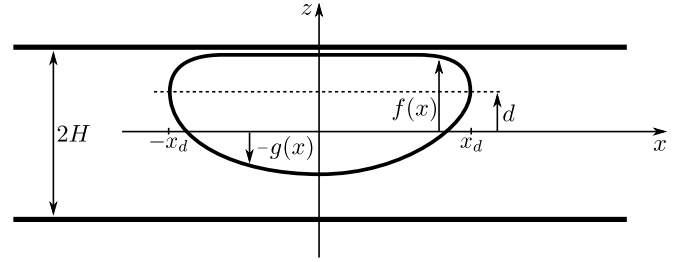


FIG. 4. The schematic shape of the A -fluid droplet deposited in a planar channel of height $2H$ and filled with B -fluid. The shape of the droplet is described by two functions: $z = f(x)$ and $z = -g(x)$ which connect smoothly at $f(x_d) = -g(x_d) = d$. We fix the symmetry axis of a droplet at $x = 0$.

The shape of a droplet can be described by two functions $z = f(x)$ and $z = -g(x)$ which connect smoothly at $z = d$ with $f'(x_d) = g'(x_d) = -\infty$. The parameter x_d is defined implicitly by equation $d = f(x_d) = -g(x_d)$. The surface free energy of the droplet per unit length in y -direction equals

$$\begin{aligned} \mathcal{H}[f, g] = \int_{-x_d}^{x_d} dx \left\{ \gamma \sqrt{1 + (f'(x))^2} + \omega(H - f(x)) - \omega(H + f(x)) \right. \\ \left. + \gamma \sqrt{1 + (g'(x))^2} + \omega(H - g(x)) - \omega(H + g(x)) \right\}, \end{aligned} \quad (5)$$

where $\omega(\ell)$ is the effective interface potential between a flat wall and the interface at a distance ℓ from it. The model of this potential stems from the microscopic density functional analysis for the one component fluid in which the attractive parts of the fluid-fluid and wall-fluid interparticle pair potentials are given by^{24–26}

$$w(r) = -\frac{A_F}{(\sigma^2 + r^2)^3}, \quad w_W(r) = -\frac{A_W}{(\sigma_W^2 + r^2)^3}, \quad (6)$$

where $A_F > 0$ and $A_W > 0$ are the amplitudes of the interactions while σ and σ_W are related to the molecular sizes of the fluid and wall particles, e.g., for argon $\sigma \approx 0.3 \text{ nm}$ ²⁷. For this model the surface tension coefficient is given by²⁸

$$\gamma = \frac{A_F \pi}{8\sigma^2} (\rho_B - \rho_A)^2, \quad (7)$$

and the effective interface potential equals

$$\omega(\ell) = \Delta\rho \frac{\pi}{4} \left[\frac{\rho_B A_F}{\sigma^2} \hat{\omega}(\ell/\sigma) - \frac{\rho_W A_W}{\sigma_W^2} \hat{\omega}(\ell/\sigma_W) \right], \quad (8)$$

where

$$\hat{\omega}(\ell) = 1 - \ell \arctan \frac{1}{\ell}. \quad (9)$$

Here $\Delta\rho = \rho_B - \rho_A$, and ρ_A, ρ_B, ρ_W are the A -fluid, B -fluid, and wall densities, respectively. After introducing dimensionless quantities

$$\hat{\rho} = \frac{1}{2} \left(1 - \frac{\rho_A}{\rho_B} \right), \quad \hat{A} = \frac{\rho_W A_W}{\rho_B A_F}, \quad \hat{\sigma}_W = \frac{\sigma_W}{\sigma} \quad (10)$$

the effective interface potential reduces to²⁸

$$\omega(\ell) = \frac{\gamma}{\hat{\rho}} \left[\hat{\omega}\left(\frac{\ell}{\sigma}\right) - \frac{\hat{A}}{\hat{\sigma}_W^2} \hat{\omega}\left(\frac{\ell}{\sigma} \frac{1}{\hat{\sigma}_W}\right) \right]. \quad (11)$$

The surface tension coefficient and the effective interface potential in Eqs (7) and (8) can be also obtained from microscopic analysis of the two-component fluid at a planar wall for specific choice of parameters characterizing the interparticle interactions, see the Appendix.

The macroscopic Young's contact angle is given by

$$\cos \theta_Y = 1 + \frac{\omega(\ell_\pi)}{\gamma}, \quad (12)$$

where $\omega(\ell_\pi)$ is the only minimum of the effective interface potential and ℓ_π is the thickness of the adsorbed layer on a planar substrate. The effective interface potential $\omega(\ell \rightarrow 0) \rightarrow \infty$, and $\omega(\ell \rightarrow \infty) \rightarrow 0$, so $\omega'(\ell < \ell_\pi) < 0$, and $\omega'(\ell > \ell_\pi) > 0$.

As the result of the minimization of the Hamiltonian under the constraint of the fixed volume A of the droplet

$$A = \int_{-x_d}^{x_d} dx \left(\bar{f}(x) + \bar{g}(x) \right) \quad (13)$$

one obtains the following equations for the equilibrium shape of the droplet $z = \bar{f}(x)$ and $z = -\bar{g}(x)$

$$\begin{aligned} \frac{\bar{f}''(x)}{(1 + \bar{f}'(x)^2)^{3/2}} &= -\bar{\omega}'(H - \bar{f}(x)) - \bar{\omega}'(H + \bar{f}(x)) - \lambda, \\ \frac{\bar{g}''(x)}{(1 + \bar{g}'(x)^2)^{3/2}} &= -\bar{\omega}'(H - \bar{g}(x)) - \bar{\omega}'(H + \bar{g}(x)) - \lambda, \end{aligned} \quad (14)$$

where λ is the Lagrange multiplier, and $\bar{\omega}(\ell) = \omega(\ell)/\gamma$. After one integration we obtain (we skip the bars)

$$\begin{aligned} \frac{1}{\sqrt{1 + f'(x)^2}} &= -\omega(H - f(x)) + \omega(H + f(x)) + \lambda f(x) + C_1, \\ \frac{1}{\sqrt{1 + g'(x)^2}} &= -\omega(H - g(x)) + \omega(H + g(x)) + \lambda g(x) + C_2. \end{aligned} \quad (15)$$

The boundary conditions:

$$\begin{aligned} f(x_d) &= -g(x_d) = d, \\ f'(x=0) &= g'(x=0) = 0, \\ f'(x_d) &= g'(x_d) = -\infty \end{aligned} \quad (16)$$

give

$$\begin{aligned} \lambda &= \frac{f_0 \eta(f_0) + g_0 \eta(g_0)}{f_0 + g_0}, \\ C_1 &= -C_2 = \frac{f_0 g_0}{f_0 + g_0} (\eta(f_0) - \eta(g_0)), \\ d\eta(d) - 1 &= \lambda d + C_1, \end{aligned} \quad (17)$$

where $f_0 = f(x=0)$, $g_0 = g(x=0)$, and $\eta(z) = (1 + \omega(H-z) - \omega(H+z))/z$. In the case of symmetric droplet, i.e. $g_0 = f_0$, the parameter $\eta(f_0)$ becomes equal to the Lagrange multiplier.

Inserting the parameters λ , C_1 , C_2 , and d as function of f_0 and g_0 into Eq. (15)

$$\begin{aligned} \frac{1}{\sqrt{1 + f'(x)^2}} &= 1 - f(x)\eta(f(x)) + \lambda f(x) + C_1, \\ \frac{1}{\sqrt{1 + g'(x)^2}} &= 1 - g(x)\eta(g(x)) + \lambda g(x) + C_2. \end{aligned} \quad (18)$$

one gets the equation

$$\int_d^{f_0} \frac{df}{|f'(x)|} = \int_{-d}^{g_0} \frac{dg}{|g'(x)|} = x_d, \quad (19)$$

which renders the values of $g_0 = g_0(f_0)$. Thus the equilibrium shape of the asymmetric droplet for a fixed volume A , Eq. (13), can be parametrized by one parameter, e.g. f_0 which is a function of the volume $f_0 = f_0(A)$.

B. Symmetric droplet

Typical droplet shapes encountered in droplet microfluidics correspond to the lengths of the droplets which are much larger than the channel height. Then the droplet is symmetric with respect to the plane parallel to the walls and located at the channel's center^{1,2}. However, there are situations, e.g. in the flow-focusing method of droplet formation in which the droplet is symmetrically deposited in channel and doesn't touch the sidewalls¹. In this section we discuss the shapes of such symmetric droplets. In particular, we investigate the dependence of the contact angle and the thickness of the films spanned between the walls and the droplet on the channel height.

For given macroscopic contact angle θ_Y , Eq. (1), and the channel height $2H$, the volume A determines the shape of the droplet. In the symmetric case one has $g_0 = f_0$ and Eqs (13) and (18) give the following relation

$$A = f_0^{3/2} \int_0^1 dt \frac{u(f_0, t)}{\sqrt{(\eta(t f_0) - \eta(f_0))}}, \quad (20)$$

where

$$u(f_0, t) = \sqrt{t} \frac{1 - f_0 t (\eta(t f_0) - \eta(f_0))}{\sqrt{2 - f_0 t (\eta(t f_0) - \eta(f_0))}}. \quad (21)$$

The function $u(f_0, t)$ is finite for $t \in [0, 1]$. The Lagrange multiplier $\eta(f_0)$ is positive for $f_0 > 0$ and has a minimum at $f_0 = f_m$ denoted as $\eta_m = \eta(f_0 = f_m)$, see Fig. 5.

For $t \rightarrow 1$

$$\begin{aligned} \eta(t f_0) - \eta(f_0) &= -f_0 \eta'(f_0)(1 - t) \\ &+ \frac{1}{2} f_0^2 \eta''(f_0)(1 - t)^2 + \dots, \end{aligned} \quad (22)$$

and it follows from Eq. (20) that $A \rightarrow \infty$ for $f_0 \rightarrow f_m$. Thus for given height of the channel, the minimal thickness of the film between the droplet and the wall $\ell_m = H - f_m$ is attained as $A \rightarrow \infty$. One can check that $\ell_m < \ell_\pi$, where ℓ_π fulfills $\omega'(\ell_\pi) = 0$, and for increasing H the minimal film thickness behaves as

$$\ell_m = \ell_\pi - \frac{\cos \theta_Y}{\omega''(\ell_\pi)} \frac{1}{H} + \mathcal{O}\left(\frac{1}{H^2}\right), \quad (23)$$

see Fig. 6.

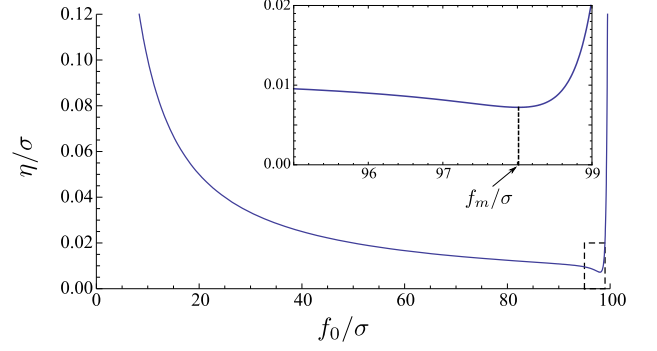


FIG. 5. The Lagrange multiplier $\eta(f_0)$ as a function of f_0 for $H = 100\sigma$. The inset shows the close-up of $\eta(f_0)$ near its minimum at $f_0 = f_m$. The surface tension coefficient and the effective interface potential parameters are chosen such that $\theta = \pi/4$ and $\ell_\pi = 2\sigma$.

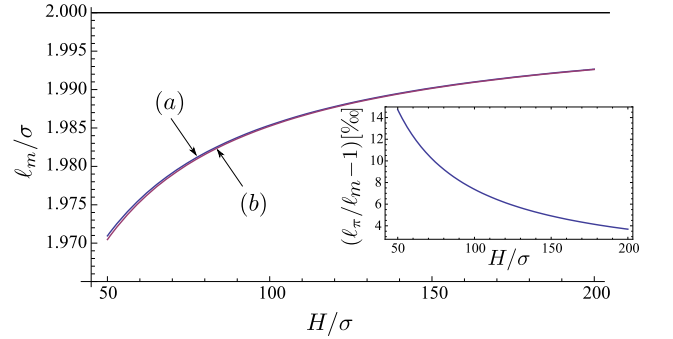


FIG. 6. The minimal film thickness ℓ_m (curve (a)) and its approximation (curve (b)), Eq. (23), as function of H for $A \rightarrow \infty$. The inset shows the relative difference between the ℓ_π and ℓ_m . The surface tension coefficient and the effective interface potential parameters are such that $\theta_Y = \pi/4$ and $\ell_\pi = 2\sigma$.

Macroscopically, the apparent contact angle of the symmetric droplet in the lenticular state is given by

$$\cos \theta_Y = \frac{H}{R}, \quad (24)$$

where R is the radius of curvature of the droplet, and H is at the same time one half of the channel's height and the highest position of the droplet interface. In mesoscopic description, we define the contact angle in the same way, and as the radius of curvature we take the inverse of a curvature at $z = 0$

$$\begin{aligned} \cos \theta &= f_0 (\eta(f_0) + 2\omega'(H)) \\ &= 1 + \omega(H - f_0) - \omega(H + f_0) + 2\omega'(H)f_0. \end{aligned} \quad (25)$$

The effective interface potential $\omega(z) \propto 1/z^2$ for $z \gg 1$, so for large H/σ and $A \rightarrow \infty$ the mesoscopic contact

angle behaves as

$$\begin{aligned} \cos \theta &= 1 + \omega(\ell_m) - \omega(2H - \ell_m) + 2\omega'(H)(H - \ell_m) \\ &= \cos \theta_Y + \frac{\cos^2 \theta_Y}{2\omega''_\pi(\ell_\pi)} \frac{1}{H^2} \\ &\quad - \omega(2H) + 2\omega'(H)H + \mathcal{O}\left(\frac{1}{H^3}\right), \end{aligned} \quad (26)$$

see Fig. 7,

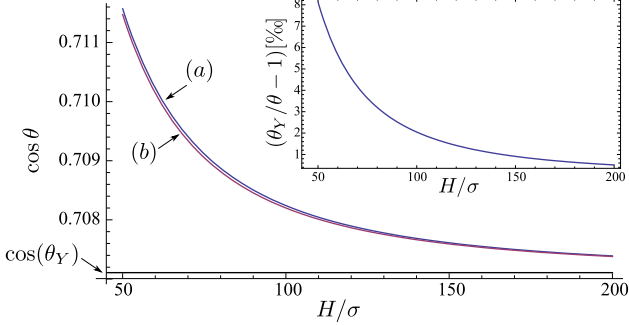


FIG. 7. The cosine of mesoscopic contact angle θ (curve (a)) and its approximation (curve (b)), Eq. (26), as function of H for $A \rightarrow \infty$. The inset shows the relative difference between the contact angle of the droplet and the Young's angle. The surface tension coefficient and the effective interface potential parameters are such that $\theta_Y = \pi/4$ and $\ell_\pi = 2\sigma$.

C. Morphological transition

The free energy profile Ω as function of volume A obtained in the mesoscopic analysis is shown on Fig. 8.

The points marked with: tr_{02} , tr_{12} , sp_0 , sp_1 , and sp_2 denote the transition and spinodal points. The circular, sessile and lenticular states cease to exist for points (A_{sp0}, Ω_{sp0}) , (A_{sp1}, Ω_{sp1}) , and (A_{sp2}, Ω_{sp2}) , respectively. The lines connecting the spinodal points correspond to unstable states. We notice that for $A > A_{sp1}$ the droplets of asymmetric shapes cannot exist in a flat channel.

The droplet profiles fulfill Eq. (15) and can be parametrized by f_0 , and g_0 – the highest and lowest position of the interface; for symmetric droplets $g_0 = f_0$. For both the circular – lenticular, and the sessile – lenticular transitions the stable and metastable states are characterized by an increasing f_0 and g_0 as a function of A , Fig. 9.

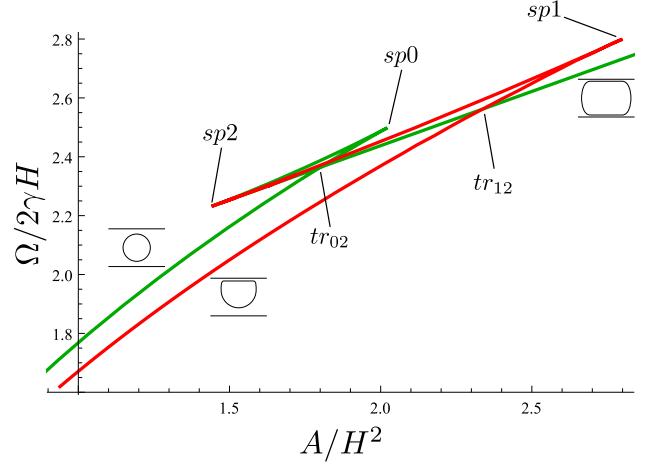


FIG. 8. Surface energy Ω as function of volume A for symmetric (green line) and asymmetric (red line) shapes for $\theta_Y = \pi/4$. The points tr_{02} , tr_{12} , sp_0 , sp_1 , and sp_2 denote the transition and spinodal points. The surface tension coefficient and the effective interface potential parameters are such that $\ell_\pi = 2\sigma$, and $H = 50\sigma$.

We notice that as soon as the lenticular state is attained the parameter f_0 remains practically constant; it doesn't increase more than 0.1σ , see also Fig. 6. Upon increasing the volume of the droplets A there is a jump in f_0 and g_0 at the transition points, Fig. 10.

In the circular state the distance between the droplet surface and the wall is large enough such that the effective interaction between the wall and the droplet surface has no effect on the shape of the droplet. In mesoscopic analysis the situation in which the droplet surface is within the distance $\ell \approx \ell_\pi$ to the wall corresponds to the droplet-wall contact in the macroscopic description. At spinodal point sp_0 the minimal film thickness between the droplet in the circular state and the wall is much larger than ℓ_π ; also for the sessile state sp_1 the distance $H - g_0 \gg \ell_\pi$, Fig. 10. For spinodal point sp_2 the mesoscopic shape resembles its macroscopic counterpart.

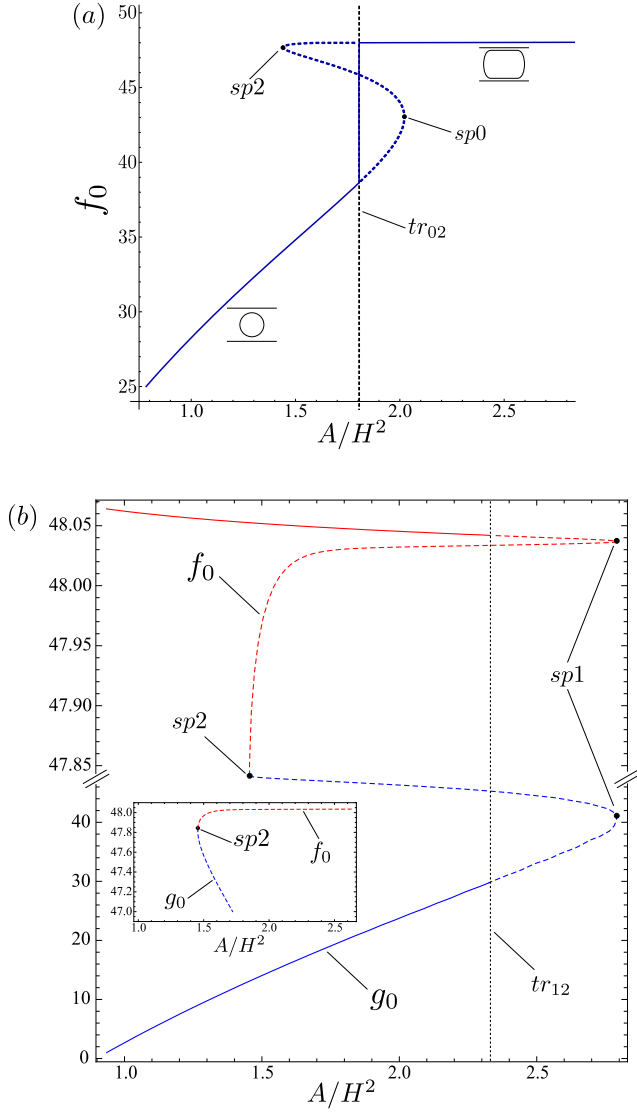


FIG. 9. The highest f_0 and the lowest g_0 positions of the droplet surface as function of the volume A for circular – lenticular, (a), and sessile – lenticular, (b), transitions. In (b) we do not display the lenticular branch which is the same as in (a). The solid lines correspond to stable states, and dashed lines to the metastable and unstable states. The transition points are marked with tr_{02} , tr_{12} , and the spinodal points with sp_0 , sp_1 and sp_2 at which the dashed lines connect smoothly, see the inset in (b). The surface tension coefficient and the effective interface potential parameters are such that $\theta_Y = \pi/4$ and $\ell_\pi = 2\sigma$, and $H = 50\sigma$.

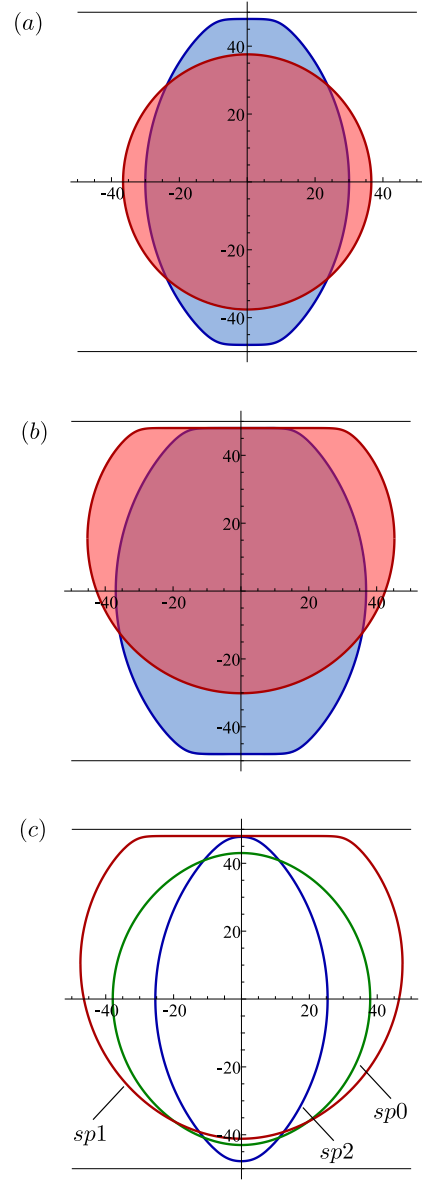


FIG. 10. The equilibrium shapes of the droplets in the circular – lenticular, (a), and the sessile – lenticular, (b), transitions at $A = A_{tr02}$ and $A = A_{tr12}$, respectively. Part (c) shows the droplet shapes at spinodal points sp_0 , sp_1 , and sp_2 . The surface tension coefficient and the effective interface potential parameters are such that $\theta_Y = \pi/4$ and $\ell_\pi = 2\sigma$, and $H = 50\sigma$.

IV. LINE TENSION

We have already noticed that the mesoscopic circular states have the same energy as the macroscopic ones. On the other hand the mesoscopic sessile and lenticular states have a lower free energy as compared to their macroscopic counterparts. The mesoscopic free energy, beside the contribution scaling with the surface of the droplet, contains also a line contribution connected with two (in the sessile state) and four (in the lenticular state) three-phase contact lines extending in the y -direction²⁹. This line contribution was not taken into account in the macroscopic description. For long-ranged van der Waals forces rendering continuous wetting transition and exploited in our analysis the line tension coefficient is negative³⁰. The formula for the line tension coefficient contains various contributions among which the most significant one includes the interaction of the solid wall with the interface detaching from the wall. According to Eq. (4.4) in Ref. 30 it takes the form

$$\tau = \frac{1}{\tan \theta_Y} \int_{\ell_\pi}^{\infty} \omega(y), \quad (27)$$

and contributes roughly to one half of the value of the line tension coefficient. Although the authors in Ref. 30 analyzed the behavior of line tension in the vicinity of wetting temperature, where $\theta_Y \rightarrow 0$, we use 2τ as the estimate of the line contribution to the free energy stemming from a single three-phase contact line, also away from the wetting point.

The inclusion of the line tension into the macroscopic description results in the change of the value of the volume A at which the morphological transitions take place. It can be calculated by solving equations

$$\begin{aligned} \Omega_0(A) &= \Omega_2(A) + 8\tau \\ \Omega_1(A) + 4\tau &= \Omega_2(A) + 8\tau \end{aligned} \quad (28)$$

for the circular – lenticular, and the sessile – lenticular transitions, respectively. In the case of the circular – lenticular transition the values of A_{tr} and Ω_{tr} characterizing the morphological phase transition calculated within the mesoscopic description are well approximated by the values obtained within the macroscopic description with the inclusion of the line tension contributions, Fig. 11.

In the case of the sessile – lenticular transition this procedure leads to results presented on Fig. 12. The line tension calculated in the full mesoscopic description turns out to be smaller (more negative) than the approximate value 2τ used within this simple approach.

The parameter f_0 characterizing the lenticular state, and therefore the contact angle θ (Eq. (25)), remain practically independent of the area A . For the values of the

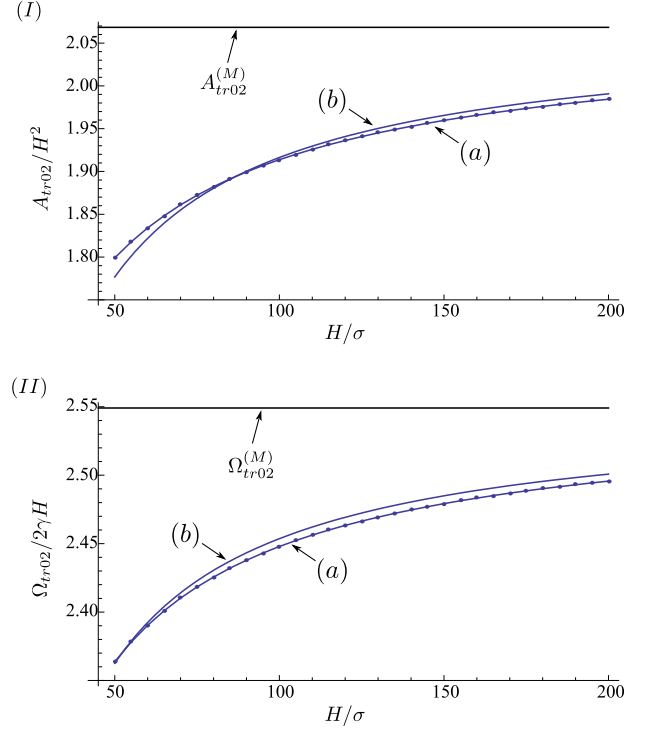


FIG. 11. The volume (I) and free energy (II) of the circular – lenticular transition as function of H obtained within mesoscopic description, (a), and macroscopic description including the line tension contributions, (b). The values of the volume and macroscopic free energy at morphological phase transition without taking into account the line tension are marked with superscripts (M).

thermodynamic and geometric parameters considered in our analysis, and for $H > 50\sigma \approx 15\text{ nm}$, Fig. 7, the Young's contact angle is a very good approximation of the mesoscopic contact angle. The relative difference is smaller than one per million. The line tension coefficient makes between 3% – 0.5% of the total free energy for H within $50\sigma - 200\sigma$. One could thus expect that the macroscopic description without including the line tension contributions would predict the values of the volume at the phase transition to be located within similar error margin, i.e. below 3%. However, this is not the case and the difference between the macroscopic and mesoscopic description is more pronounced, between 5% – 14%, Fig. 13.

The relative difference $A_{tr}^{(M)}/A_{tr} - 1$ between the volume at the circular – lenticular transition within macroscopic description without including the line tension contributions ($A_{tr}^{(M)}$) and mesoscopic description (A_{tr}) decreases like $1/H$, as expected. In case of the sessile – lenticular transition the numerical results are less reliable due to numerical errors induced by solving Eq. 19 and calculating the droplet shape and its free energy in the sessile state.

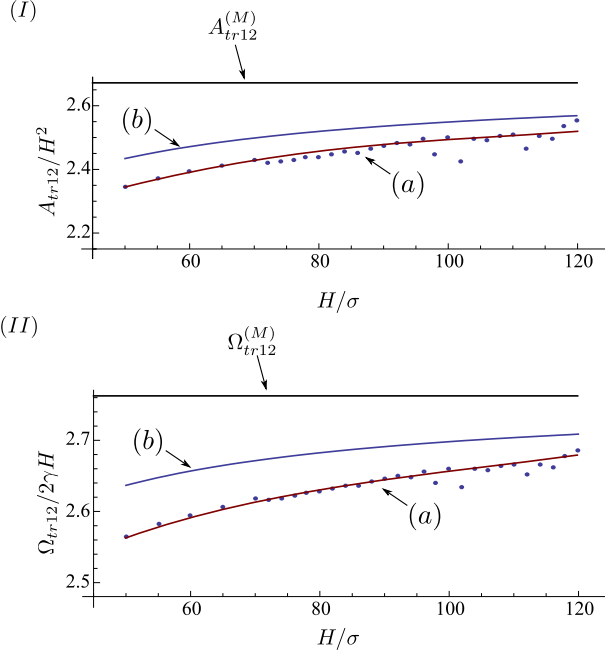


FIG. 12. The volume (I) and free energy (II) of the sessile – lenticular transition as function of H obtained within mesoscopic description, (a), and macroscopic description including the line tension contributions, (b). The values of the volume and the macroscopic free energy at morphological phase transition including the line tension are marked with superscripts (M).

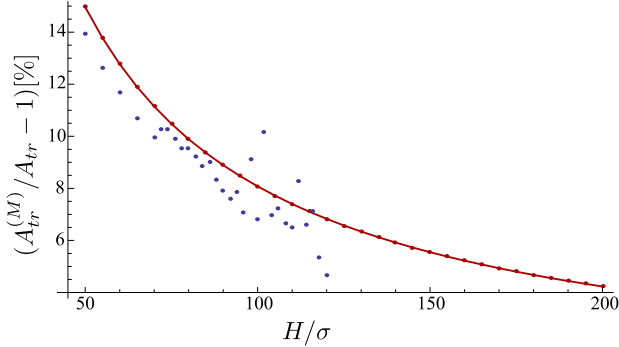


FIG. 13. The relative difference between the volume at the circular – lenticular (red dots), and the sessile – lenticular (blue dots) transitions within macroscopic approach without taking into account the line tension, $A_{tr}^{(M)}$, and mesoscopic approaches, A_{tr} .

V. SOLVATION FORCE

Insertion of the A -fluid droplet into the channel filled by the B -fluid changes the free energy of the system

and, in particular, modifies the solvation force acting between the sidewalls. The solvation force F is calculated as $F = -\partial\Omega/\partial(2H)$ at fixed volume of the droplet.

In macroscopic description only the free energy of the lenticular state depends on the channel height, Eq. (2). The solvation force per unit length in the y -direction is thus non-zero and equals²⁰

$$\begin{aligned} F^{(M)} &= -\frac{\partial\Omega_2}{\partial(2H)} = \gamma \left(\frac{1}{2} \cos \theta_Y \frac{A}{H^2} - \frac{\pi - 2\theta_Y}{2 \cos \theta_Y} - \sin \theta_Y \right) \\ &= \frac{\gamma}{R} (2d - 2R \sin \theta_Y) = 2d\Delta p - 2\gamma \sin \theta_Y, \end{aligned} \quad (29)$$

where $2d$ is the length of the droplet-wall interface, R is the radius of curvature of AB interface, and $\Delta p = p_A - p_B = \gamma/R$ is the Laplace pressure, see Fig. 14.

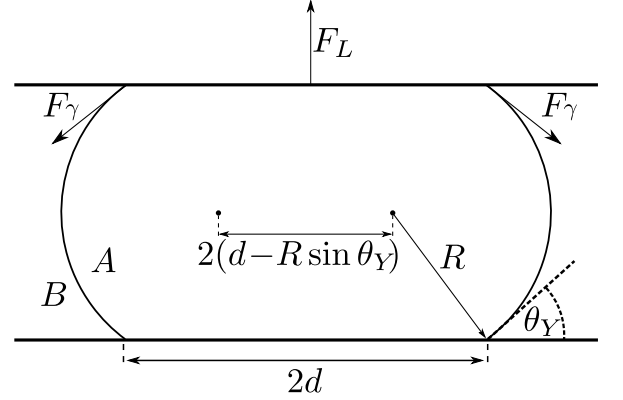


FIG. 14. Schematic shape of the droplet in macroscopic description of the lenticular state. The length of the droplet-wall interface is denoted by $2d$, the radius of curvature of the $A - B$ interface by R , and the contact angle by θ_Y . The solvation force (per unit length in the y -direction) acting on the upper wall contains contribution from the Laplace force $F_L = 2d\Delta p = 2d\gamma/R$, where Δp is the Laplace pressure, and the surface tension contribution denoted by $F_\gamma = \gamma$.

Accordingly, the solvation force is positive when the center of each arc of the circle forming the AB interface (points O_1 and O_2 in Fig. 14) and the corresponding interface are located on the same side of the droplet symmetry axis perpendicular to the channel walls. Upon increasing the channel height the solvation force decreases and becomes zero when the arcs centers O_1 and O_2 merge on the symmetry axis, and becomes negative for larger values of H , Fig. 15. We notice that - for larger values of H - the lenticular state becomes metastable against the sessile or circular state. In particular, for large enough channel height one has $2d = 0$, and the lenticular state ceases to exist.

In mesoscopic description, the free energy of the lenticular state, Eq. (5), is given by

$$\mathcal{H}[\bar{f}] = 4 \int_0^{x_d} dx \left\{ \gamma \sqrt{1 + (\bar{f}'(x))^2} + \omega(H - \bar{f}(x)) - \omega(H + \bar{f}(x)) \right\}, \quad (30)$$

where $z = \bar{f}(x)$ describes the equilibrium shape of the droplet. Correspondingly, the solvation force is given by

$$\begin{aligned} F &= - \frac{\partial \mathcal{H}[\bar{f}]}{\partial(2H)} = - \frac{1}{2} \frac{\partial \mathcal{H}[\bar{f}]}{\partial H} \\ &= - 2 \int_0^{x_d} dx \left\{ \omega'(H - \bar{f}(x)) - \omega'(H + \bar{f}(x)) \right\}. \end{aligned} \quad (31)$$

In agreement with the macroscopic analysis conclusions the solvation force is positive for small values of the channel height and becomes negative for larger values, Fig. 16. For decreasing H the thickness of the film between the droplet and the wall, $\ell_0 = H - f_0$ decreases and the derivative $\omega'(\ell_0)$ becomes more negative; therefore the solvation force can be positive. For higher values of H the thickness ℓ_0 increases, $\omega'(\ell_0)$ becomes less negative and the solvation force changes its sign.

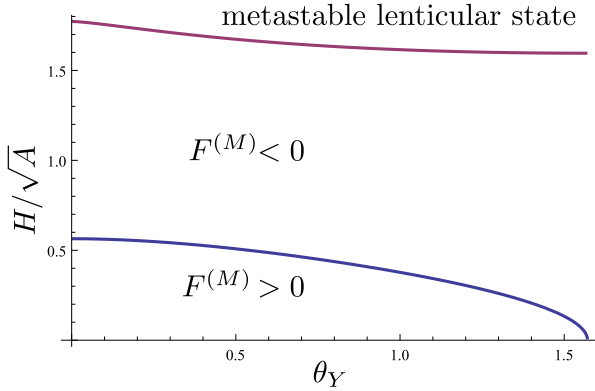


FIG. 15. The diagram in (θ_Y, H) variables illustrating the change of sign of the solvation force in the case of macroscopically analyzed lenticular state at fixed volume A . The red line denotes the sessile-lenticular transition above which the lenticular state is metastable.

The shape of the droplet corresponding to $F = 0$ is such that the radius of curvature R of the droplet at $z = 0$ equals x_d , $R = x_d$. In this situation, the $A - B$ interface can be approximated by two arcs of the same circle with the center at $(x = 0, z = 0)$, Fig. 17.

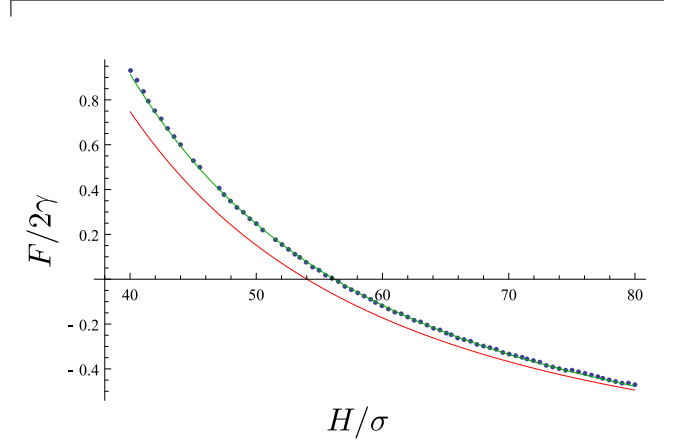


FIG. 16. The solvation force F as a function of H calculated within mesoscopic (dots) and macroscopic (red line) analysis. The green line is introduced to guide the eye. The calculation was done for $A = 15000\sigma^2$; the surface tension coefficient γ and the effective interface potential parameters are such that $\theta_Y = \pi/4$ and $\ell_\pi = 2\sigma$.

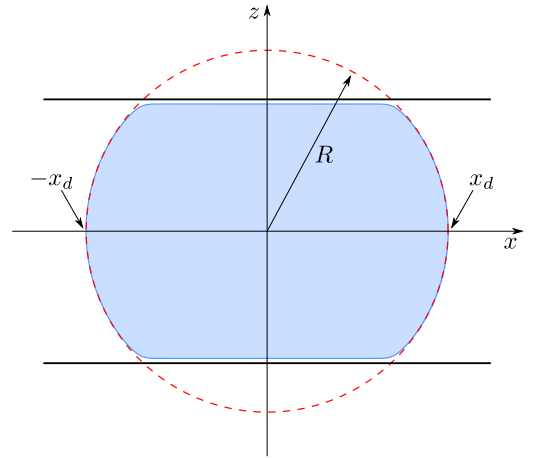


FIG. 17. The shape of the mesoscopic droplet corresponding to zero solvation force, $F = 0$. The shape of the droplet is such that the radius of curvature of the interface R at $z = 0$ equals x_d , and the $A - B$ interface can be approximated by two arcs of the same circle with the center at $(x = 0, z = 0)$. The droplet shape corresponding to $F^{(M)} = 0$ in the macroscopic analysis also exhibits this feature.

VI. DISCUSSION

We have derived the phase diagrams for the circular-lenticular and the sessile-lenticular morphological transitions of a droplet in a channel within two approaches: macroscopic and mesoscopic. Since the free energy of the sessile state is always smaller than that of the circular state the former transition can be observed only when droplet configurations which are symmetric with respect to the center plane of a channel are imposed on the system. e.g., via the appropriate constraint. Both morphological transitions are first-order and are accompanied by the presence of metastable and unstable states. In mesoscopic description the free energy profile, Fig. 8, is qualitatively the same as in the macroscopic description, Fig. 3. However, the macroscopic approach which is not corrected by the inclusion of the line tension contributions, overestimates both the free energies and volumes at transition points up to 14% as compared to the mesoscopic values, see Fig. 13. This comparison can be substantially improved by including the contact angle dependent line tension coefficient, Figs. 11, 12.

The long-ranged interparticle interactions taken into account in analysis, Eq. (6), render the critical wetting transition at a planar substrate and lead to negative line tension coefficient. The interparticle interactions leading to the first-order wetting transition give positive line tension coefficient^{29,31}. We suppose that in this case the values of volumes characterizing the sessile –lenticular transition will be larger than in the case of negative line tension coefficients. In addition to the transition points, also the spinodal points would change within the macroscopic description including the line tension contributions. Thus the analysis of the droplet states in the nanochannels can give us a hint about the underlying interparticle interaction and the order of the wetting transition.

In the mesoscopic description there is always a layer of the host B -fluid separating the A -fluid droplet from the channel walls. This is the most profound difference between the mesoscopic description and its macroscopic counterpart, where one allows for the droplet-wall interface. Nevertheless, also in the mesoscopic approach one can define the contact angle θ , see Eq. (25). This angle approaches the macroscopic Young's angle θ_Y for $H \rightarrow \infty$ and droplet's volume $A \rightarrow \infty$. For mesoscopic channel heights and large droplets ($A \rightarrow \infty$) this angle is smaller than θ_Y , Fig. 7. The difference $\theta_Y - \theta$ decreases with increasing height and its relative value is smaller than one per mil already for $H = 50\sigma$.

In the mesoscopic description of the lenticular states of large droplets the film thickness between the droplet and the wall $\ell_0 = H - f_0$ is smaller than ℓ_π , i.e., the thickness of the adsorption layer of the B -fluid on a planar substrate, Fig. 6. The difference $\ell_\pi - \ell_0$ decreases with increasing channel height and for $H > 50\sigma$ it is smaller than 0.05σ . However, even this minor difference give rise to the positive (repulsive) solvation force, which is also

present in macroscopic description. Approximating ℓ_0 by ℓ_π would incorrectly render the always negative (attractive) solvation force, see Eq. (31).

The predicted change of sign of the solvation force in the lenticular state, also reported in Refs. 19 and 20, brings new issue in experimental micro- and nanofluidics. Suppose that one wall of the channel filled with the B -fluid can move in the direction perpendicular to it. Inserting many identical droplets of the A -fluid of fixed volume (with large enough distance between them to prevent their coalescence) will determine the distance between the walls of the channel. This height is a function of number and the volume of the inserted droplets. Generally, the droplets of the A -fluid immersed in the channel filled with the B -fluid can act as micro- or nanodampers (shock absorbers).

Appendix: Effective interaction between a flat wall and droplet surface

Consider an interface fluctuating near a planar wall, see Fig. 18. This interface separates the phases A and B rich in components 1 and 2, respectively. The thermodynamic state of the system corresponds to the coexistence of these A and B phases of the binary mixture. The system is invariant in y -direction and $z = f(x)$ denotes the position of the interface. The interfacial Hamiltonian

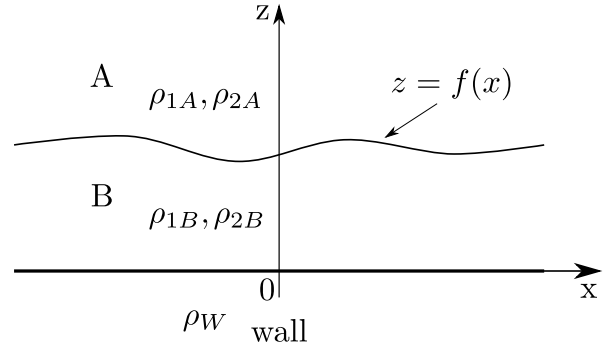


FIG. 18. The two-component system at a planar substrate. The system is invariant in y -direction and $z = f(x)$ is a fluid-fluid interface separating phases A , and B rich in component 1 and 2, respectively.

takes the form^{32,33}

$$\mathcal{H}_{AB}[f] = \int_{-\infty}^{\infty} dx \left\{ \gamma_{AB} \sqrt{1 + (f'(x))^2} + \omega_{AB}(f(x)) \right\} \quad (\text{A.1})$$

where γ_{AB} is the surface tension coefficient, and $\omega_{AB}(\ell)$ is the effective interface potential between the wall and the interface located at the distance ℓ from it. We con-

sider the following model of long-ranged attractive interparticle $w_{ij}(r)$ and wall-particle $w_{iW}(r)$ interactions

$$w_{ij}(r) = -\frac{A_{ij}}{(\sigma_{ij}^2 + r^2)^3}, \quad w_{iW}(r) = -\frac{A_{iW}}{(\sigma_{iW}^2 + r^2)^3}, \quad (\text{A.2})$$

where $i, j = 1, 2$ enumerate the fluid components. The amplitudes A_{ij} and A_{iW} are positive; the positive parameters σ_{ij} and σ_{iW} are related to the molecular sizes of the fluid and substrate particles. For this model the surface tension coefficient is equal

$$\gamma_{AB} = \frac{\pi}{8} \sum_{i,j=1}^2 \frac{A_{ij}}{\sigma_{ij}^2} (\rho_{iB} - \rho_{iA})(\rho_{jB} - \rho_{jA}), \quad (\text{A.3})$$

and the effective interface potential

$$\omega_{AB}(\ell) = \frac{\pi}{4} \sum_{i,j=1}^2 (\rho_{iB} - \rho_{iA}) \left(\rho_{jB} \frac{A_{ij}}{\sigma_{ij}^2} \hat{\omega}(\ell/\sigma_{ij}) - \rho_W \frac{A_{iW}}{\sigma_{iW}^2} \hat{\omega}(\ell/\sigma_{iW}) \right), \quad (\text{A.4})$$

where ρ_{iA} , ρ_{iB} denote the number density of i th component in phases A and B , ρ_W is the density of the wall, and

$$\hat{\omega}(\ell) = 1 - \ell \arctan \frac{1}{\ell}. \quad (\text{A.5})$$

For the following choice of the amplitudes and molecular sizes³⁴

$$A_{ij} = \sqrt{A_{ii}A_{jj}}, \quad A_{iW} = \sqrt{A_{ii}A_{WW}} \quad (\text{A.6})$$

$$\sigma = \sigma_{ij}, \quad \sigma_W = \sigma_{iW}, \quad i, j = 1, 2$$

the surface tension coefficient and the effective interface potential can be rewritten as

$$\gamma_{AB} = \frac{\pi}{8\sigma^2} \left(\sum_{i=1}^2 \sqrt{A_{ii}} (\rho_{iB} - \rho_{iA}) \right)^2$$

$$\omega_{AB}(\ell) = \frac{\pi}{4} \left(\sum_{i=1}^2 \sqrt{A_{ii}} (\rho_{iB} - \rho_{iA}) \right) \left(\sum_{j=1}^2 \frac{\rho_{jB} \sqrt{A_{jj}}}{\sigma^2} \hat{\omega}(\ell/\sigma) - \frac{\rho_W \sqrt{A_{WW}}}{\sigma_W^2} \hat{\omega}(\ell/\sigma_W) \right). \quad (\text{A.7})$$

Upon introducing the dimensionless quantities

$$\hat{\rho}_{AB} = \frac{1}{2} \left(1 - \frac{\sum_{i=1}^2 \sqrt{A_{ii}} \rho_{iA}}{\sum_{i=1}^2 \sqrt{A_{ii}} \rho_{iB}} \right),$$

$$\hat{A}_{AB} = \frac{\rho_W \sqrt{A_{WW}}}{\sum_{i=1}^2 \sqrt{A_{ii}} \rho_{iB}}, \quad (\text{A.8})$$

$$\hat{\sigma}_W = \frac{\sigma_W}{\sigma}$$

the effective interface potential reduces to

$$\omega_{AB}(\ell) = \frac{\gamma_{AB}}{\hat{\rho}_{AB}} \left[\hat{\omega}_{AB} \left(\frac{\ell}{\sigma} \right) - \frac{\hat{A}_{AB}}{\hat{\sigma}_W^2} \hat{\omega}_{AB} \left(\frac{\ell}{\sigma} \frac{1}{\sigma_W} \right) \right], \quad (\text{A.9})$$

which is exactly the form of the effective interface potential for the one component system, see Eqs (11) and (61) in Ref. 28.

ACKNOWLEDGMENTS

F.D. was supported by Foundation for Polish Science within the project Homing Plus/2012-6/3, co-financed from European Regional Development Fund. M.N. acknowledges support from the National Science Center via grant 2011/03/B/ST3/02638.

- ¹T. Squires and S. Quake, "Microfluidics: Fluid physics at the nanoliter scale," *Rev. Mod. Phys.* **77**, 977–1026 (2005).
- ²R. Seemann, M. Brinkmann, T. Pfohl, and S. Herminghaus, "Droplet based microfluidics," *Rep. Prog. Phys.* **75**, 016601 (2012).
- ³P. G. de Gennes, F. Brochard-Wyart, and D. Quere, *Capillarity and wetting phenomena: drops, bubbles, pearls, waves* (Springer: London, 2004).
- ⁴D. Bonn, J. Eggers, J. Indekeu, J. Meunier, and E. Rolley, "Wetting and spreading," *Rev. Mod. Phys.* **81**, 739–805 (2009).
- ⁵H. Wong, S. Morris, and C. Radke, "2-dimensional menisci in nonaxisymmetric capillaries," *J. Colloid Interface Sci.* **148**, 284–287 (1992).
- ⁶H. Wong, S. Morris, and C. Radke, "3-dimensional menisci in polygonal capillaries," *J. Colloid Interface Sci.* **148**, 317–336 (1992).
- ⁷V. S. Ajaev, *Interfacial Fluid Mechanics: A Mathematical Modeling Approach* (Springer, 2012).
- ⁸P. Kim, H.-Y. Kim, J. K. Kim, G. Reiter, and K. Y. Suh, "Multicurvature liquid meniscus in a nanochannel: Evidence of interplay between intermolecular and surface forces," *Lab Chip* **9**, 3255–3260 (2009).
- ⁹L. Shui, A. van den Berg, and J. C. T. Eijkel, "Scalable attoliter monodisperse droplet formation using multiphase nanomicrofluidics," *Microfluid. Nanofluid.* **11**, 87–92 (2011).
- ¹⁰C. M. Megaridis, A. G. Yazicioglu, J. A. Libera, and Y. Gogotsi, "Attoliter fluid experiments in individual closed-end carbon nanotubes: Liquid film and fluid interface dynamics," *Phys. Fluids* **14**, L5–L8 (2002).
- ¹¹D. Mattia and Y. Gogotsi, "Review: static and dynamic behavior of liquids inside carbon nanotubes," *Microfluid. Nanofluid.* **5**, 289–305 (2008).
- ¹²V. S. Ajaev and G. M. Homsy, "Steady vapor bubbles in rectangular microchannels," *J. Colloid Interface Sci.* **240**, 259–271 (2001).
- ¹³V. S. Ajaev and G. M. Homsy, "Three-dimensional steady vapor bubbles in rectangular microchannels," *J. Colloid Interface Sci.* **244**, 180–189 (2001).
- ¹⁴V. S. Ajaev and G. M. Homsy, "Modeling shapes and dynamics of confined bubbles," in *Annual Review of Fluid Mechanics*, Vol. 38 (Annual Reviews, Palo Alto, 2006) pp. 277–307.
- ¹⁵J. W. van Honschoten, N. Brunets, and N. R. Tas, "Capillarity at the nanoscale," *Chem. Soc. Rev.* **39**, 1096–1114 (2010).
- ¹⁶V. M. Starov, "Surface forces action in a vicinity of three phase contact line and other current problems in kinetics of wetting and spreading," *Advances in Colloid and Interface Science* **161**, 139–152 (2010).
- ¹⁷D. Mattia, V. Starov, and S. Semenov, "Thickness, stability and contact angle of liquid films on and inside nanofibres, nanotubes and nanochannels," *J. Colloid Interface Sci.* **384**, 149–156 (2012).

- ¹⁸M. Fortes, “Axisymmetric liquid bridges between parallel plates,” *J. Colloid Interface Sci.* **88**, 338–352 (1982).
- ¹⁹E. J. De Souza, M. Brinkmann, C. Mohrdieck, A. Crosby, and E. Arzt, “Capillary forces between chemically different substrates,” *Langmuir* **24**, 10161–10168 (2008).
- ²⁰H. Kusumaatmaja and R. Lipowsky, “Equilibrium morphologies and effective spring constants of capillary bridges,” *Langmuir* **26**, 18734–18741 (2010).
- ²¹D. J. Broesch and J. Frechette, “From concave to convex: Capillary bridges in slit pore geometry,” *Langmuir* **28**, 15548–15554 (2012).
- ²²H.-J. Butt and M. Kappl, *Surface and Interfacial Forces* (John Wiley & Sons, 2009).
- ²³F. Dutka and M. Napiórkowski, “The influence of line tension on the formation of liquid bridges in atomic force microscope-like geometry,” *J. Phys.-Condes. Matter* **19** (2007).
- ²⁴M. Tasinkevych and S. Dietrich, “Complete wetting of nanosculptured substrates,” *Phys. Rev. Lett.* **97**, 106102 (2006).
- ²⁵M. Tasinkevych and S. Dietrich, “Complete wetting of pits and grooves,” *Eur. Phys. J. E* **23**, 117 (2007).
- ²⁶T. Hofmann, M. Tasinkevych, A. Checco, E. Dobisz, S. Dietrich, and B. Ocko, “Wetting of nanopatterned grooved surfaces,” *Phys. Rev. Lett.* **104**, 106102 (2010).
- ²⁷J.-P. Hansen and L. Verlet, “Phase transitions of the Lennard-Jones system,” *Phys. Rev.* **184**, 151–161 (1969).
- ²⁸F. Dutka, M. Napiórkowski, and S. Dietrich, “Mesoscopic analysis of gibbs’ criterion for sessile nanodroplets on trapezoidal substrates,” *J. Chem. Phys.* **136** (2012).
- ²⁹L. Schimmele, M. Napiórkowski, and S. Dietrich, “Conceptual aspects of line tensions,” *J. Chem. Phys.* **127**, 164715 (2007).
- ³⁰T. Getta and S. Dietrich, “Line tension between fluid phases and a substrate,” *Phys. Rev. E* **57**, 655 (1998).
- ³¹J. Indekeu, “Line tension near the wetting transition - results from an interface displacement model,” *Physica A* **183**, 439–461 (1992).
- ³²S. Dietrich and M. Napiórkowski, “Analytic results for wetting transitions in the presence of vanderwaals tails,” *Phys. Rev. A* **43**, 1861–1885 (1991).
- ³³T. Hiester, S. Dietrich, and K. Mecke, “Microscopic theory for interface fluctuations in binary liquid mixtures,” *J. Chem. Phys.* **125**, 184701 (2006).
- ³⁴F. Dutka, M. Napiórkowski, and S. Dietrich, “Effective hamiltonian for fluid membranes in the presence of long-ranged forces,” *Phys. Rev. E* **78** (2008).